SCIENTIFIC REPORTS
natureresearch

OPEN

Precise determination of surface band bending in Ga-polar n-GaN films by angular dependent X-Ray photoemission spectroscopy

Yanfei Zhao[1*], Hongwei Gao[2], Rong Huang[1], Zengli Huang[1], Fangsen Li[1], Jiagui Feng[1], Qian Sun[2], An Dingsun[1*] & Hui Yang[1,2]

We present a systematic study of surface band bending in Ga-polar n-GaN with different Si doping concentrations by angular dependent X-ray photoelectron spectroscopy (ADXPS). The binding energies of Ga 3d and N 1s core levels in n-GaN films increase with increasing the emission angle, i. e., the probing depth, suggesting an upward surface band bending. By fitting the Ga 3d core level spectra at different emission angles and considering the integrated effect of electrostatic potential, the core level energy at the topmost surface layer is well corrected, therefore, the surface band bending is precisely evaluated. For moderately doped GaN, the electrostatic potential can be reflected by the simply linear potential approximation. However, for highly doped GaN samples, in which the photoelectron depth is comparable to the width of the space charge region, quadratic depletion approximation was used for the electrostatic potential to better understand the surface band bending effect. Our work improves the knowledge of surface band bending determination by ADXPS and also paves the way for studying the band bending effect in the interface of GaN based heterostructures.

Group III-nitrides and related alloys have received considerable research interests in recent years mainly due to their advantages in high power/high speed device applications[1–4]. Large spontaneous and piezoelectric polarization effects in Gallium Nitride (GaN) induce large band bending in surface layer and also across the interface of the heterojunction[5]. Surface band bending plays an important role in semiconductor devices by modifying the basic electronic properties and efficiency of them[6]. The effective electron surface band bending results from the complex superposition of contributions from localized surface state charges and polarization charges in wurtzite GaN crystal, and directly affects the device performance[7]. It has been reported that heavily Si doped GaN ohmic layers, in lateral contact to two-dimensional electron gas in the GaN channel, could dramatically improve the DC and RF characteristics in GaN-high electron mobility transistors (GaN-HEMT)[8]. However, there have been few reports on studying the surface band bending in GaN with different doping density, especially in highly doped GaN films. Therefore, it is highly desirable to precisely determine the surface band bending in different doped GaN, to reveal the complication in physics of semiconductor device.

Angular dependent X-ray photoelectron spectroscopy (ADXPS) has been used as a surface sensitive method to determine the surface band bending[9–11]. By decreasing the photoelectron emission angle θ respected to the sample surface, the surface sensitivity of the photoelectron spectroscopy can be increased since the detection depth of photoelectron reduces by a factor of $\sin(\theta)$[12]. Thus, the magnitude of surface band bending can be obtained by measuring the change of photoelectron spectra at different emission angles. However, when considering the real situation of a surface with band bending, the collected core level photoelectron peak is actually an integration of photoelectrons coming from several subsurface atomic layers, instead of the topmost surface layer. In the band bending assessment, the magnitude of surface band bending is determined by the difference in core level energies at the topmost atomic layer and the corresponding value in the bulk, while, the measured photoelectron peak without deconvolution function at the topmost surface layer is expected to be shifted due to

[1]Vacuum Interconnected Nanotech Workstation (Nano-X), Suzhou Institute of Nano-Tech and Nano-Bionics (SINANO), Chinese Academy of Sciences (CAS), Suzhou, 215123, China. [2]Key Laboratory of Nanodevices and Applications, Chinese Academy of Sciences (CAS), Suzhou, 215123, China. *email: yfzhao2015@sinano.ac.cn; adingsun2014@sinano.ac.cn

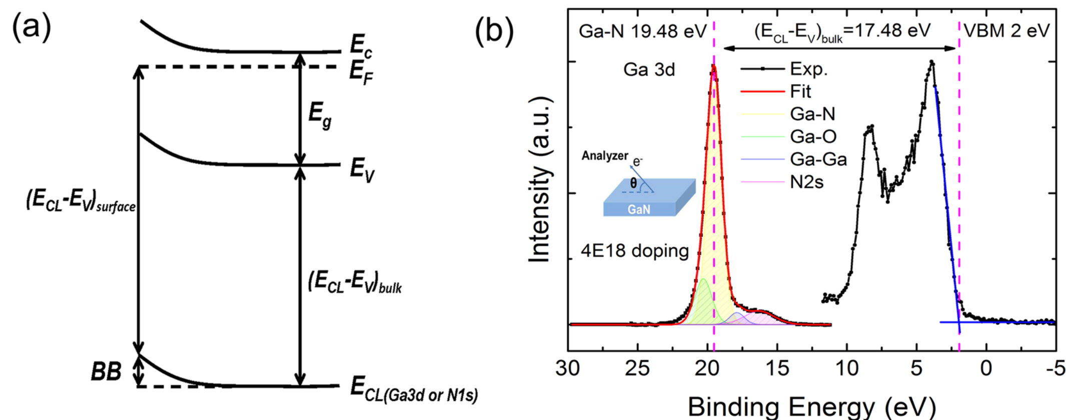

Figure 1. Surface band bending calculation in Ga-polar n-GaN films. (**a**) Schematic surface band bending in Ga-polar n-GaN. (**b**) The measured Ga 3d core level and valance band spectrum of S2 at $\theta = 85°$ are shown by black dots and lines. The Ga 3d spectrum can be fitted into four peaks. The Ga-N, Ga-O, Ga-Ga bonds and N2s peaks are displayed by the yellow, green, blue, magenta lines respectively. The red line represents the fitting envelope. The magenta dashed lines are eye-guides to show the peak position of the Ga-N bond and VBM. The inset shows the definition of emission angle θ .

the integral effect, which may lead an underestimate or overestimate of the band bending extent[13–15]. To improve the accuracy of analysis, we derive the actual photoelectron peak from different detection depth by performing a method of peak deconvolution to eliminate the integrating effect caused by electrostatic potential. After deconvolution function correction, the actual core level binding energy dependence on the detection depth can be obtained, improving the accuracy of the band bending assessment. In this paper, Ga-polar n-GaN samples with different Si doping densities have been studied by using ADXPS. Ga 3d core level spectra were evaluated correctly by considering the band bending due to the electrostatic potential affected by the doping density combined with localized charges on the surface. In the case of moderate Si doping GaN films, the electrostatic potential can be evaluated simply by a linear relationship to the depth by deconvolution correction. While, in heavily Si doped case, due to the steep space charge potential, the quadratic depletion approximation is more reasonable than linear potential approximation in the surface band bending deconvolution calculation. With deconvolution correction, the surface band bending in different doping density GaN films are precisely determined.

Results and Discussion

A schematic band diagram for the surface band bending measurement is outlined in Fig. 1(a). The surface band bending (BB) in GaN can be determined from core level binding energy, such as, Ga 3d or N 1 s, and other inherent properties of GaN, as described in the following[6,9]:

$$\text{Band bending(BB)} = (E_{CL} - E_V)_{\text{bulk}} + E_g - E_C - (E_{CL} - E_V)_{\text{surface}} \quad (1)$$

where, $(E_{CL} - E_V)_{\text{bulk}}$ is the binding energy difference between core level and valance band maxima in GaN bulk which is a material constant, E_g is the band gap of GaN (3.45 eV[16]), E_C is the position of conduction band with respect to the Fermi level, and depends on doping concentration, $(E_{CL} - E_V)_{\text{surface}}$ is the core level energy referenced to the Fermi level energy on GaN surface, which would change with the doping density and the surface states. For comparison, three kinds of Si doped GaN films were studied, with doping level of $9 \times 10^{17}\,\text{cm}^{-3}$ (sample 1), $4 \times 10^{18}\,\text{cm}^{-3}$ (sample 2) and $1.4 \times 10^{19}\,\text{cm}^{-3}$ (sample 3), respectively. The doping densities are verified by secondary ion mass spectroscopy (SIMS) measurements. For sample 1 (S1), E_c is calculated to be 0.03 eV above the Fermi level. When the doping density increases, the Fermi level moves to a higher level. E_c is calculated to be 0.03 eV and 0.1 eV below the Fermi level for sample 2 (S2) and sample 3 (S3).

Figure 1(b) shows the XPS spectra of the Ga 3d core level spectra, as well as the valance band of S2, collected at emission angle of $\theta = 85°$ and represented as black dots and lines. By taking Shirley background subtraction and a combination of Gaussian and Lorentzian line shapes, the Ga 3d spectrum can be fitted into four peaks, corresponding to the Ga-N, Ga-O, Ga-Ga bonds and N2s. The fitted highest peak at 19.48 eV originates from Ga-N bond. The valance band maximum (VBM) is determined by the intercept of the slope at the leading edge of the valance band spectrum with the base line, shown by the blue solid line in Fig. 1(b). The energy difference of $(E_{CL} - E_V)_{\text{bulk}}$ is calculated to be 17.48 eV, which is consistent with the values reported for bulk GaN[17–20].

Figure 2(a–c) show the Ga 3d core level spectra at different emission angles in different Si doped GaN samples. As displayed in Fig. 2(a), the characteristic Ga $3d_{(\text{Ga-N})}$ peak in S1 shifts toward higher energy with increasing the emission angle θ. Actually, the photoelectron escape depth depends on the emission angle (θ) in a simple relation of $\lambda \sin(\theta)$, where λ is the inelastic mean free path of photoelectrons. The value of λ is 2.6 nm for photoelectrons of Ga 3d in GaN, as calculated by TPP-2M method[21] in NIST's database[22]. Thus, the binding energy of Ga $3d_{(\text{Ga-N})}$ peak increases monotonically with the increase of detection depth (about 3λ), as shown in the insert of Fig. 2, implying a sharp upward band bending exists in the GaN surface layer. The similar upward band bending phenomena can also be clearly observed in the Ga 3d $_{(\text{Ga-N})}$ peaks in S2 and S3, as shown in Fig. 2(b,c), respectively.

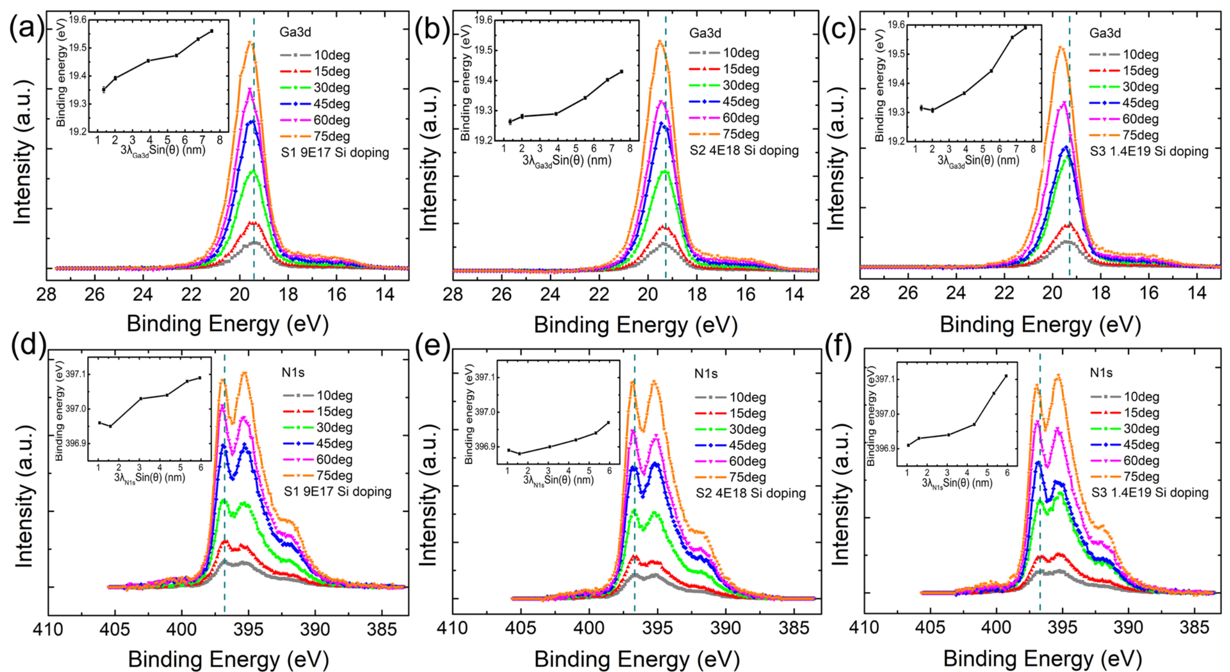

Figure 2. Measured core level spectra of different Si doped GaN samples. (**a–c**) Ga 3d core level spectra measured at different emission angle θ for S1, S2 and S3. The inset displays the binding energy of Ga $3d_{(Ga\text{-}N)}$ peak as a function of detection depth. (**d–f**) N 1 s core level spectra measured at different detection angle θ for S1, S2 and S3, respectively. The inset displays the binding energy of N 1 $s_{(N\text{-}Ga)}$ peak as a function of detection depth. The green dashed lines are eye-guides to highlight the variation of peak position.

Moreover, the peak shift extent of the highly doped sample (S3) is larger than that of S1 and S2, indicating a larger equivalent internal electric filed exists in S3. It is noted that similar binding energy shift can be also observed in the spectra of N 1 s peaks of different Si doped GaN samples, as shown in Fig. 2(d–f).

As reported previously[5], an internal potential gradient exists in GaN material due to its large spontaneous polarization. The spontaneous polarization of Ga-polar n-GaN would lead to negative surface bound charges, while the positive donor charges formed in n-GaN compensate the polarization-induced negative surface charge and form an electron accumulation layer, which induces an upward band bending[6]. As shown in Fig. 1(a), the core level (E_{CL}), the VBM (E_v) and the conduction band minimum (E_c) all bent upward in the Ga-polar n-GaN surface layer. It is known that a core level spectrum obtained by ADXPS is an integration of photoelectrons emitter within the detection depth of the topmost surface. As schematically outlined in Fig. 3, the measured spectrum without deconvolution shown by the solid black line is an integration of the actual spectrum at each depth point along the bend core level displayed by the dash dot color lines. Namely, the dash dot color lines performed the deconvoluted spectra at different depth point. Due to the exponential decay of the XPS intensity, it is educible that the contribution of photoelectrons emitted from a deeper layer is overwhelmed by the contribution of photoelectrons from a shallower layer, leading the peak energy position shifts away from the original binding energy due to the effect of integration. In other words, for an electronic band structure with upward bending, the measured maximum of the integrated photoelectron peak without deconvolution is expected to be shifted away from the deconvoluted binding energy at that depth, guided by the dashed black lines in Fig. 3, and thus gives an under- or overestimation on the band bending magnitude from the values on the very surface.

Based on the ADXPS core level peaks collected at different emission angles, we derive the dependence of photoelectron binding energy on depth in the undersurface layer by taking a method of peak deconvolution for eliminating the integrated effect caused by electrostatic potential. Briefly, a measured core level spectrum as a function of the binding energy, is given as follows[23]:

$$I(E) = \int_0^{\infty} I_0(E - \psi(z))\exp\left(-\frac{z}{\lambda \sin\theta}\right)dz \tag{2}$$

where, z is the depth from the surface of the bulk, $I_0(E)$ refers to the typical core level spectrum with a peak energy of E. $\psi(z)$ stands for the assumed electrostatic potential. λ is the inelastic mean free path of photoelectrons. Here, $I_0(E-\psi(z))$ can be expressed by the pseudo-Voigt function[24]:

$$I_0(E - \psi(z)) = I_{00}\left[\alpha \exp\left(-\ln 2\frac{(E - \psi(z))^2}{(F/2)^2}\right) + (1 - \alpha)\frac{1}{1 + \frac{(E - \psi(z))^2}{(F/2)^2}}\right] \tag{3}$$

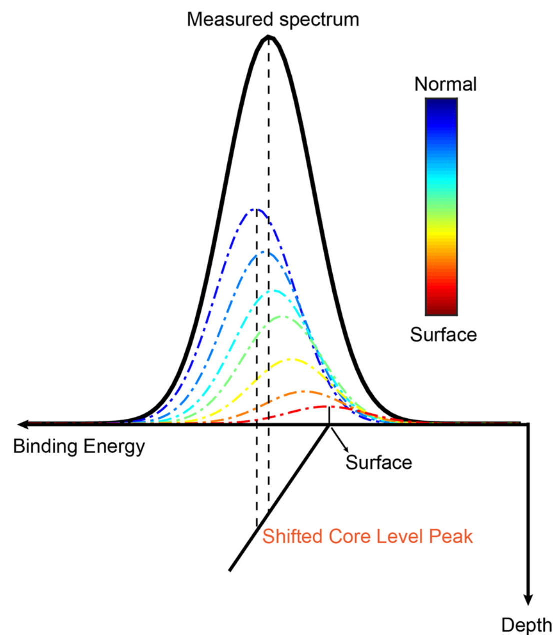

Figure 3. Schematic explaining the deconvolution of the spectra by ADXPS. The shifted core level peak refers to the discrepancy between the measured and actual peak energy position due to the effect of band bending.

where, I_{00}, α, and F are the core level spectrum intensity, the ratio of Gaussian function, and the full width at half maximum (FWHM) of the core level spectrum, respectively. As shown in Fig. 4, the measured binding energies of Ga 3d $_{\text{(Ga-N)}}$ peak are plotted by black solid circles as a function of detection depth. The blue dashed lines are eye-guides to show the peak positions of the binding energies that shift with the detection depth in a linear way, indicating the surface band bending existing in all three samples. However, the peak position of each spectrum collected at different emission angles actually represent the integrated contribution of photoelectrons from different detection depth to sample surface. To figure out the actual binding energy of photoelectron emitted from a certain depth, it is necessary to deintegrate the measured peak according to Eqs (2, 3). First, we consider a uniform internal potential gradient on the surface of Ga-polar n-GaN and $\psi(z)$ is a linear relationship to z. By deconvolution of the spectra measured at different emission angles, we obtained the dependence of the actual core level binding energy on the detection depth, shown by the red dashed lines in Fig. 4. The calculated binding energy at surface E_0, is summarized in Table I. For comparison, the binding energy at the topmost surface layer by the linear fitting of the measured data without deconvolution is expressed by E_s.

As shown in Table I, by assuming a linear surface potential $\psi(z)$ in GaN, the discrepancy between E_0 and E_s values are small for S1 and S2, which is consistent with the XPS theory that the major photoemission contribution origins from the topmost atomic layers and the deconvolution affects little at the topmost surface. However, in S3 with higher doping density, E_s shifts away from E_0, indicating the inaccuracy of linear potential approximation. For S1 and S2, the space charge region width is dozens of nanometer, which is much larger than the detection depth, so we adopt the linear potential approximation at the surface (details are shown in the supplementary information). Owing to the high doping level in S3, the width of the space charge region is reduced to be comparable with the photoelectron depth, thus the realistic quadratic depletion approximation should be more suitable.

To gain further insights in highly doped GaN sample, the quadratic depletion approximation correction was considered. In the depletion approximation, $\psi(z)$ was treated as $\psi(z) \approx \psi_s\left(1 - \sqrt{\frac{qN_d}{2\varepsilon_{GaN}\psi_s}}z\right)^2$, where ψ_s is the surface potential at $z = 0$, q is the electronic charge, N_d is the doping density, and ε_{GaN} is the dielectric constant of GaN[25]. As shown in Fig. 5(a), the experimentally observed Ga 3d spectra measured at different emission angles were quantitatively in agreement with the quadratic depletion approximation fitting (black dashed lines). The extracted binding energy at topmost surface, E_0, is 19.30 eV. The actual core level binding energy as a function of detection depth after considering the effect of quadratic depletion approximation by Eqs (2, 3) is shown by the green dashed line in Fig. 5(b). Compared with the linear potential approximation (red dashed line in Fig. 5(b)), the deviation between E_0 and E_s becomes smaller. The quadratic depletion approximation is closer to the experimental results in surface layers.

To sum up, for the moderately doped GaN, due to the larger depletion width, the effective electron surface potential can be reflected by the simply linear approximation, while in highly doped GaN, the quadratic depletion approximation is more applicable. Moreover, by calculating the surface band bending, according to Eq. (1), the surface band bending for three different doping densities after deconvolution correction are calculated to be 1.53 eV, 1.72 eV, and 1.73 eV for S1, S2 and S3 respectively.

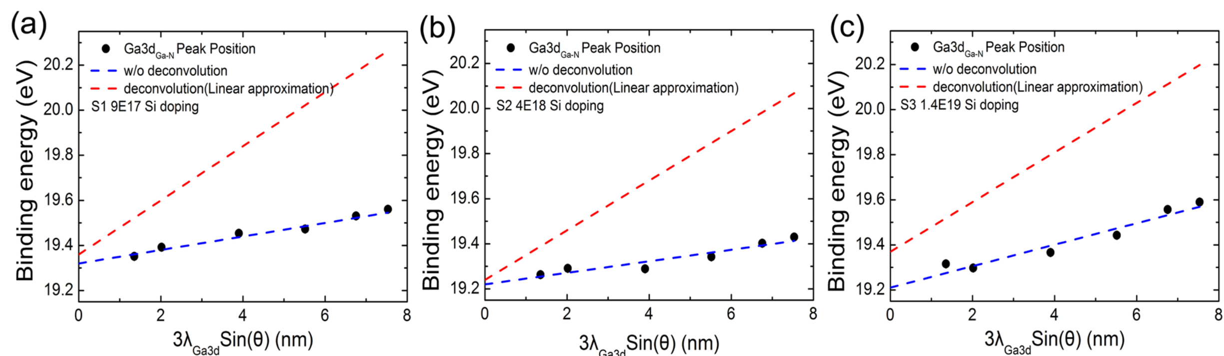

Figure 4. The binding energy of Ga 3d $_{(Ga\text{-}N)}$ peak as a function of detection depth with carrier concentration of (**a**) $9 \times 10^{17}\,cm^{-3}$ (S1), (**b**) $4 \times 10^{18}\,cm^{-3}$ (S2) and (**c**) $1.4 \times 10^{19}\,cm^{-3}$ (S3). The blue dashed lines are eye-guides to show the linear fitting of the measured binding energy. The red dashed lines exhibit the actual core level binding energy as a function of detection depth after considering the effect of linear electrostatic potential by Eqs (2, 3).

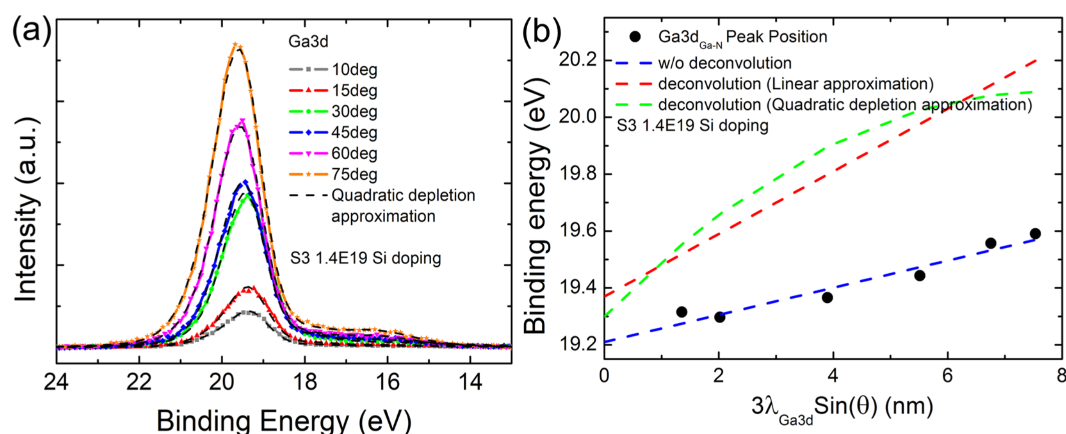

Figure 5. Quadratic depletion approximation correction in highly Si doped GaN films (S3). (**a**) The experimentally observed Ga 3d spectra of S3 at different emission angles are shown by solid symbol- lines. The black dashed lines are the fittings using the quadratic depletion approximation by Eqs (2, 3). (**b**) The binding energy of Ga 3d $_{(Ga\text{-}N)}$ peak as a function of detection depth with carrier concentration of $1.4 \times 10^{19}\,cm^{-3}$ (S3). The blue dashed lines are the linear fitting of the measured binding energy peak without deconvolution. The red dashed line performed the deconvolution of the spectra by linear approximation and the green dashed lines show the deconvolution of the spectra by quadratic depletion approximation.

	Doping density (cm^{-3})	$(E_{CL} - E_F)_{surface}$			Band bending (eV)
		w/o deconvolution E_s	Linear approximation E_0	Quadratic approximation E_0	
S1	9×10^{17}	19.32	19.37	/	1.53 (Linear)
S2	4×10^{18}	19.22	19.24	/	1.72 (Linear)
S3	1.4×10^{19}	19.21	19.38	19.30	1.73 (Quadratic)

Table I. The values of $(E_{CL} - E_V)_{surface}$ without (w/o) deconvolution and deconvolution by linear approximation as well as the quadratic depletion approximation, and band bending of different doping density GaN samples.

Conclusion

In summary, we performed a systematic study on the surface band bending of Ga-polar n-GaN with different Si doping density via ADXPS. The binding energies for Ga 3d and N 1 s in GaN films increase with increasing the detection depth, implying an upward surface band bending. Considering the effect of integration caused by internal electric field in band bending samples, we corrected the core level binding energies by subtracting the integrated effect and correctly determined the value of surface band bending. Our study confirms the major contributions come from the surface layers. For moderately doped GaN, the effective electron surface potential can be represented by a simply linear approximation. For highly doped GaN, where the photoelectron emission

depth is comparable to the width of the space charge region, a quadratic depletion approximation should be adapt to simulate the internal potential distribution with band bending effect.

Methods

Sample Preparation. Three different Si doped Ga-polar n-GaN films with thickness of 1μm were grown on 2-inch p-type Si (111) substrates with undoped GaN buffer layers of 1.5 μm in between by metal organic chemical vapor deposition. The carrier concentrations of the three samples are in the range of (8.5–9.5) $\times 10^{17}\,cm^{-3}$ for Sample 1, $4 \times 10^{18}\,cm^{-3}$ for Sample 2, and $1.4 \times 10^{19}\,cm^{-3}$ for Sample 3, as characterized by using Hall measurement and verified by secondary ion mass spectroscopy (SIMS).

ADXPS characterization. ADXPS was carried out by using a PHI 5000 Versaprobe II system equipped with a monochromatic Al Kα (1486.6 eV) X-ray source, to obtain the core level and valance band structure spectra of all samples. The core level spectra were subtracted by a Shirley-type background and fitted using combined Gaussian and Lorentzian line shapes. The valance band maxima were determined by extrapolating a linear fit of the leading edge of the valance band photoemission to the baseline. The binding energy calibration was performed by using gold (Au), silver (Ag), and copper (Cu) standard samples by setting Au $4f_{7/2}$, Ag $3d_{5/2}$, Cu $2p_{3/2}$ peaks at binding energies of 83.96 ± 0.1 eV, 368.21 ± 0.1 eV and 932.62 ± 0.1 eV, respectively. The XPS spectra were performed at different emission angles θ from 10° to 85°, with respect to the sample surface, ranging. The Fermi edge was calibrated using a pure and *in-situ* cleaned silver (Ag) standard sample and setting the binding energy at 0.00 eV. To further calibrate the charging effect, the spectra were referenced to the peak position of C1s core levels to 284.8 eV for each sample.

TOF-SIMS characterization. The concentration of doped Si in n-GaN were verified by a TOF-SIMS depth profile technique, using a Bi+ ion beam with energy of 30 keV and pulsed current of 3.5 pA for analysis. Depth sputtering was performed using a Cs+ beam of 2 keV and 75 nA to produce a crater of 200×200 μm. The analysis area was 50×50 μm in the center of the crater. Si- ions were collected at negative ion detection mode.

Received: 11 April 2019; Accepted: 29 October 2019;

Published online: 18 November 2019

References

1. Bermudez, V. M. The fundamental surface science of wurtzite gallium nitride. *Surf. Sci. Rep.* **72**, 147–315 (2017).
2. Ponce, F. A. & Bour, D. P. Nitride-based semiconductors for blue and green light-emitting devices. *Nature* **386**, 351–359 (1997).
3. Schubert, E. F. & Kim, J. K. Solid-state light sources getting smart. *Science* **308**, 1274–1278 (2005).
4. Krames, M. R. *et al.* Status and future of high-power light-emitting diodes for solid state lighting. *J. Display Tech.* **3**, 160–175 (2007).
5. Ambacher, O. *et al.* Two-dimensional electron gases induced by spontaneous and piezoelectric polarization charges in N- and Ga-face AlGaN/GaN heterostructures. *J. Appl. Phys.* **85**, 3222–3333 (1999).
6. Bartoš, I. *et al.* Electron band bending of polar, semipolar and non-polar GaN surfaces. *J. Appl. Phys.* **119**, 105303 (2016).
7. Yang, J., Eller, B. S. & Nemanich, R. J. Surface band bending and band alignment of plasma enhanced atomic layer deposited dielectrics on Ga- and N-face gallium nitride. *J. Appl. Phys.* **116**, 123702 (2014).
8. Shinohara, K. *et al.* Self-aligned-gate GaN-HEMTs with heavily-doped n^+-GaN ohmic contacts to 2DEG. 2012 International Electron Devices Meeting. 27.2.1-27.2.4 (2012).
9. Eller, B. S., Yang, J. & Nemanich, R. J. Polarization Effects of GaN and AlGaN: Polarization Bound Charge, Band Bending, and Electronic Surface States. *J. Electron. Mater.* **43**, 4560–4568 (2014).
10. Duan, T. L., Pan, J. S. & Ang, D. S. Investigation of Surface Band Bending of Ga-Face GaN by Angle-Resolved X-ray Photoelectron. *Spectroscopy. ECS J. Solid State Sci. Technol.* **5**, 514–517 (2016).
11. Akazawa, M. *et al.* Measurement of valence-band offsets of InAlN/GaN heterostructures grown by metal-organic vapor phase epitaxy. *J. Appl. Phys.* **109**, 013703 (2011).
12. Paynter, R. W. An ARXPS primer. *J. Electron. Spectrosc. Relat. Phenom.* **169**, 1–9 (2009).
13. Bartoš, I. *et al.* Electron band bending and surface sensitivity: X-ray photoelectron spectroscopy of polar GaN surfaces. *Surf. Sci.* **664**, 241–245 (2017).
14. Margaritondo, G., Gozzo, F. & Coluzza, C. Band bending at semiconductor interfaces and its effect on photoemission line shapes. *Phys. Rev. B* **47**, 9907–9909 (1993).
15. Xu, X. *et al.* Influence of band bending and polarization on the valence band offset measured by x-ray photoelectron spectroscopy. *J. Appl. Phys.* **107**, 104510 (2010).
16. Paisley, M. J. *et al.* Growth of cubic phase gallium nitride by modified molecular-beam epitaxy. *J. Vac. Sci. Technol. A* **7**, 701–705 (1989).
17. Ye, G. *et al.* Band alignment between GaN and ZrO2 formed by atomic layer deposition. *Appl. Phys. Lett.* **105**, 022106 (2014).
18. Mishra, M. *et al.* New Approach to Clean GaN. *Surfaces. Mater. Focus* **3**, 218–223 (2014).
19. Wu, C. I. *et al.* GaN (0001)-(1×1) surfaces: Composition and electronic properties. *J. Appl. Phys.* **83**, 4249–4252 (1998).
20. Huang, R. *et al.* Angular dependent XPS study of surface band bending on Ga-polar n-GaN. *Appl. Surf. Sci.* **440**, 637–642 (2018).
21. Tanuma, S., Powell, C. J. & Penn, D. R. Calculations of electron inelastic mean free paths. V. Data for 14 organic-compounds over the 50–2000 eV range. *Surf. Interface Anal.* **21**, 165–176 (1994).
22. Powell, C. J. & Jablonski, A. NIST Electron inelastic-mean-free-path database. v1.2 https://www.nist.gov/sites/default/files/documents/srd/SRD71Users GuideV1-2.pdf (2010).
23. Briggs, D. & Seah, M. P. Practical Surface Analysis by Auger and X-ray Photoelectron Spectroscopy (John Wiley & Sons Ltd, Chichester, 1983).
24. Sanchez-Bajo, F. & Cumbrera, F. L. The use of the Pseudo-Viogt Function in the variance method of X-ray Line broadening analysis. *J. Appl. Cryst*. **30**, 427-430 (1997).
25. Kraut, E. A., Grant, R. W., Waldrop, J. R. & Kowalczyk, S. P. Semiconductor core-level to valence-band maximum binding-energy differences: Precise determination by x-ray photoelectron spectroscopy. *Phys. Rev. B* **28**, 1965–1977 (1983).

Acknowledgements
The authors are grateful for the National Natural Science Foundation of China (Grant No. 61604167). We are thankful for the technical support from Platform for Nano-X of SINANO, CAS.

Author contributions
Y.Z., Z.H., A.D. and H.Y. conceived and designed the experiments. Y.Z. performed XPS experiments. H.G. grew the GaN samples. S.Q. supervised the sample growth. R.H. and F.L. performed TOF-SIMS experiment. Y.Z., R.H., Z.H., F.L., J.F. and A.D. analyzed the data. Y.Z. and A.D. wrote the manuscript.

Competing interests
The authors declare no competing interests.

Additional information
Supplementary information is available for this paper at https://doi.org/10.1038/s41598-019-53236-9.

Correspondence and requests for materials should be addressed to Y.Z. or A.D.

Reprints and permissions information is available at www.nature.com/reprints.

Publisher's note Springer Nature remains neutral with regard to jurisdictional claims in published maps and institutional affiliations.

Open Access This article is licensed under a Creative Commons Attribution 4.0 International License, which permits use, sharing, adaptation, distribution and reproduction in any medium or format, as long as you give appropriate credit to the original author(s) and the source, provide a link to the Creative Commons license, and indicate if changes were made. The images or other third party material in this article are included in the article's Creative Commons license, unless indicated otherwise in a credit line to the material. If material is not included in the article's Creative Commons license and your intended use is not permitted by statutory regulation or exceeds the permitted use, you will need to obtain permission directly from the copyright holder. To view a copy of this license, visit http://creativecommons.org/licenses/by/4.0/.

© The Author(s) 2019